JOURNAL OF GEOPHYSICAL RESEARCH, VOL. 104, NO. C1, PAGES 1343–1359, JANUARY 15, 1999

Motional induction effect on the planetary-scale geoelectric potential in the eastern North Pacific

Ikuko Fujii,[1]

Institute of Theoretical Geophysics, University of Cambridge, Cambridge, England

Alan D. Chave

Woods Hole Oceanographic Institution, Woods Hole, Massachusetts

Abstract. Geoelectric potentials induced by seawater motion on a planetary scale were studied using voltage differences measured on the Hawaii-1 (HAW-1) submarine cable between Hanauma Bay, Oahu, Hawaii, and Point Arena, California. The motionally induced field was extracted from a 3.6-year segment of the HAW-1 voltage by cancelling the component that is coherent with the externally produced geomagnetic field at Honolulu. The corrected voltage shows significant coherence with atmospheric variables (wind stress curl, wind stress, and surface pressure) estimated from the European Centre for Medium-Range Weather Forecasts product at points throughout the Pacific basin at periods from 5 to 133 days. This suggests that the voltage reflects regional to basin-wide depth-averaged (barotropic) water currents that are directly wind driven. Contour maps of the squared coherence reveal that (1) peak coherence as large as 0.6-0.8 is seen at points both near the cable and nonlocally, (2) higher coherence is seen at periods where the cable voltage power spectrum peaks, and (3) spatial patterns of the coherence vary with period. Comparison of power spectra or coherence maps for individual years shows that the wind-driven flow fluctuates temporally owing to long-term variations of the wind field. The main features of these observations are consistent with those from point electric field measurements, suggesting that planetary-scale voltages measured with cables can serve as a useful tool to monitor large-scale water currents at long periods.

1. Introduction

The motion of conductive seawater through the geomagnetic field is known to induce voltage differences within the ocean through the dynamo effect. A number of theoretical and observational studies have demonstrated that the motionally induced horizontal electric field at a point is proportional to the cross product of the known vertical component of the geomagnetic field and the vertically integrated, seawater conductivity-weighted horizontal water velocity. This yields the depth-averaged water velocity with a small error term at most points in the ocean [e.g., *Sanford*, 1971; *Chave and Luther*, 1990; *Luther et al.*, 1991; *Luther and Chave*, 1993; *Larsen*, 1992]. A submarine cable averages this quantity along its track, directly giving the transport in the absence of depth variations or when an independent calibration is available [*Larsen*, 1992; *Flosadóttir et al.*, 1997b]. Ocean bottom electrometers are being increasingly used to measure the water velocity when the depth-averaged value is of interest [e.g., *Chave et al.*, 1992a, 1997]. Similarly, the induced voltage on a submarine cable has been used to estimate the horizontal water flux (i.e., the mass transport) across the Florida Straits for more than a decade [*Larsen*, 1992].

In recent years, the availability of basin- to planetary-scale geoelectric potential measurements has rapidly increased owing to the existence of numerous decommissioned telecommunications cables in oceanic areas. Such large-scale voltage measurements differ from more conventional point measurements in several important respects. A cable will be sensitive only to the largest-scale features of the flow field because horizontal averaging of the water velocity along the cable reduces the influence of smaller-scale velocity components. Therefore cables offer the possibility of making contributions to basin- to planetary-scale oceanography and especially the study of large-scale water transport, which is complementary to other techniques. Another benefit to the

[1]Now at Earthquake Research Institute, University of Tokyo, Tokyo, Japan.

Copyright 1999 by the American Geophysical Union.

Paper number 1998JC900041.
0148-0227/99/1998JC900041$09.00

use of cables is that nearly continuous measurements are possible over the long term at very low cost.

In this study, we have examined the motionally induced voltage from a nearly 4-year-long time series of voltage differences between Hawaii and California. This is the first time that a basin-scale geoelectric potential data set covering such a long period of time has become available. *Chave et al.* [1992b] had reported that the first year of this data set was coherent with atmospheric variables at long periods, both locally (i.e., at points immediately above and around the cable) and at distant points, implying the presence of large-scale wind-driven flows. We have extended this study by using geomagnetic field data to cancel residual noise from the external geomagnetic field, thereby substantially raising the signal-to-noise ratio, and by using a much longer record. We then used surface air pressure and wind products over the entire Pacific Ocean basin to search for spatial and frequency patterns in their coherence with the cable voltage.

2. Theory

Motional induction has attracted the attention of oceanographers since *Faraday* [1832] first recognized its existence. Early experimental attempts generally gave depressing results because of technical problems and difficulties in interpretation. *Sanford* [1971] and *Chave and Luther* [1990] extended the early theoretical work of *Longuet-Higgins* [1949] and successfully developed a theory for the motionally induced electromagnetic field in the ocean. An approximate relationship between the horizontal electric field $\mathbf{E}_h$ in a flat-bottomed ocean and the horizontal water velocity $\mathbf{v}_h$ at low frequencies where self- and mutual induction effects are negligible and the horizontal length scale of the flow is large compared to the water depth and at points away from continent edges is given by

$$\mathbf{E}_h = CF_z\hat{z} \times \langle \mathbf{v}_h \rangle^* \tag{1}$$

where

$$\langle \mathbf{v}_h \rangle^* = \frac{\int_{-D}^{0} \sigma(z)\mathbf{v}_h(z)dz}{\int_{-D}^{0} \sigma(z)dz} \tag{2}$$

C is a dimensionless factor lying between 0 and 1 and typically 0.95, which gives the fraction of the induced field that does not leak into the conductive Earth, while F_z, D, and σ give the vertical geomagnetic field, the water depth, and the seawater electrical conductivity, respectively. Equation (1) means that $\mathbf{E}_h$ is proportional to the conductivity-weighted, depth-integrated flow $\langle \mathbf{v}_h \rangle^*$. Because vertical variations in σ are small, $\langle \mathbf{v}_h \rangle^*$ is dominated by the depth-averaged (hereafter referred to as barotropic) flow at most points in the ocean. This relationship has been verified observationally on numerous occasions, most recently, by using collocated point electric field sensors and moored current meters [*Luther et al.*, 1991].

For a submarine cable, (1) is integrated laterally along the cable length, and hence the voltage very nearly reflects the total amount of transport across the cable. Motionally induced fields on cables have been detected in many experiments [e.g., *Longuet-Higgins,* 1949; *Stommel,* 1954; *Cox et al.*, 1964; *Teramoto,* 1971; *Duffus and Fowler,* 1974; *Richards,* 1977; *Medford et al.*, 1981; *Mori,* 1987; *Kawatate et al.*, 1991; *Chave et al.*, 1992b; *Teramoto and Kojima,* 1994]. Until the 1970s, comparisons of these measurements with theory were not entirely successful because the studies focused on tidal components where (1) is not satisfied because self- and mutual-induction effects are significant. However, two comparatively short (100 km or less) experiments in the Straits of Florida [e.g., *Larsen and Sanford,* 1985] and the Bering Strait [*Bloom,* 1964] showed that the low-frequency cable voltage reflects water transport across it through comparison with independent observations of water velocity along the cable. This is more difficult to accomplish quantitatively for a planetary-scale submarine cable because independent transport measurements are sparse and the motionally induced signals are weaker owing to spatial averaging [*Chave et al.*, 1992b].

Interpretation problems for cable voltage measurements include the effects of nonlocal electric currents [*Sanford,* 1971; *Larsen,* 1992; *Stephenson and Bryan,* 1992], current short circuiting by a conductive seafloor [*Cox,* 1980; *Chave and Luther,* 1990], and topography [*Larsen,* 1992]. Numerical simulations have been making essential contributions to resolving these uncertainties [e.g., *Stephenson and Bryan,* 1992; *Tyler and Mysak,* 1995]. In this respect, the numerical results of *Flosadóttir et al.* [1997a, b] are especially important. They verified the validity of (1) throughout the North Atlantic basin by combining a general circulation model incorporating realistic topography with a finite difference scheme to solve the electromagnetic problem in the presence of the same topography. Their results extended the observed linear relationship between cable voltage and local transport observed in the Straits of Florida to most points in the ocean and suggested that voltages measured on planetary-scale submarine cables will reflect the water transport even at points far from boundary currents.

3. Data

The cable used for this work is Hawaii-1 (HAW-1), which extends from Hanauma Bay, Oahu, Hawaii, to Point Arena, California, as shown in Figure 1. The HAW-1 cable consists of a coaxial copper cable 3926 km long with 57 in-line repeaters and equalizers. The coaxial cable works effectively as the lead to connect distant electrodes to a recording voltmeter. The voltage difference between the center conductor, which is connected to the retired telecommunications ground system at Hanauma Bay, and a dedicated local reference

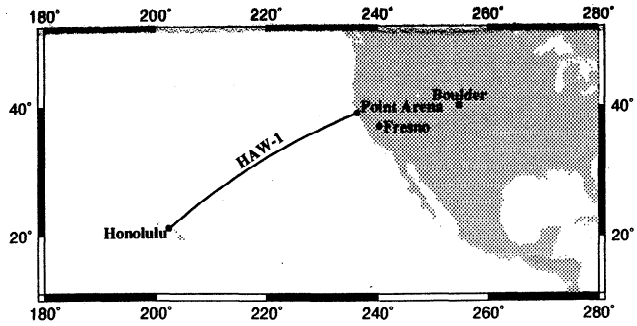

Figure 1. Location of the Hawaii-1 (HAW-1) cable and the standard geomagnetic observatories at Honolulu, Fresno, and Boulder.

ground at Point Arena was recorded at the latter site every 2 s. Details on the measuring system may be found in *Lanzerotti et al.* [1992]. This measurement program was initiated in April 1990 and continues to the present, with only infrequent, brief interruptions.

The voltage data used in this study are 20-min median values computed from the 2-s samples covering 1425 days extending from April 7, 1990, to March 2, 1994, (Figure2a). The data are dominated by large periodic signals that correspond to the ocean tide and the ionospheric solar daily variation (Sq) and its harmonics. The latter display strong seasonal effects and are not true periodic phenomena, unlike the ocean tides. Since none of these is of direct interest and they introduce analysis complexity, they were removed using a robust least squares procedure. This was applied to the voltage at the frequencies of the seven major oceanic tides (Q_1, O_1, P_1, K_1, N_2, M_2, and S_2) and the solar daily variation and harmonics at 1-8 cpd plus up to eight additional sidebands spaced at intervals of 1 cycles per year (cpy) on both sides of these frequencies to account for seasonal effects on Sq. Hourly mean values were computed by low-pass filtering and decimation after removing the sinusoidal signals. Data gaps shorter than 3 hours were interpolated using a cubic spline. The hourly voltage time series also contains 16 data gaps of 0.2- to 8.6-day duration, which were left intact, as shown in Figure 2b.

In addition to the motionally induced component, geomagnetic field fluctuations due to time-varying electric current systems in the ionosphere and magnetosphere are present in the cable data. There are several reports on features of the externally induced field on this cable [e.g., *Lanzerotti et al.*, 1992, 1993; *Chave et al.*, 1992b; *Lizarralde et al.*, 1995]. The HAW-1 voltage is dominated by the externally induced field at periods shorter than several days and affected by it to periods of 10-20 days. Therefore we filled data gaps in excess of 3 hours long using a relationship between the cable voltage and the geomagnetic field at nearby standard magnetic observatories. Hourly mean values of the geomagnetic field at Honolulu (HON)(21.3°N, 202.0°E), Fresno (FRN)(37.1°N, 240.3°E), and Boulder (BOU)(40.1°N, 254.8°E) were obtained from the U.S.Geological Survey. These geomagnetic observatories are shown in Figure 1.

The procedure used here is described by *Chave et al.* [1992b] and *Lizarralde et al.* [1995] and is similar to that given by *Egbert* [1992]. First, the vector transfer function between a gappy data set and a reference data set is estimated in the frequency domain using a robust algorithm with leverage control. Second, the transfer function is converted to a vector finite impulse response in the time domain using an inverse approach that requires that the transfer function corresponding to the impulse response be smooth in a well-defined way and also fit the estimates at a prescribed misfit level. Finally, missing data are estimated by convoluting the impulse response with the reference data. Because there are gaps in the magnetic field data from the three observatories (2.8%, 0.5%, and 0.5% of the total, respectively), the procedure was first applied to the geomagnetic field at FRN referred to the BOU data, then to the HON data referred to the filled FRN data, and finally to the HAW-1 voltage referred to the filled HON data. Figure 2c shows the hourly mean values of HAW-1 with the gaps filled. This procedure is reasonable because (1) the amount of missing data is small, (2) the duration of each gap is not too long, and (3) the

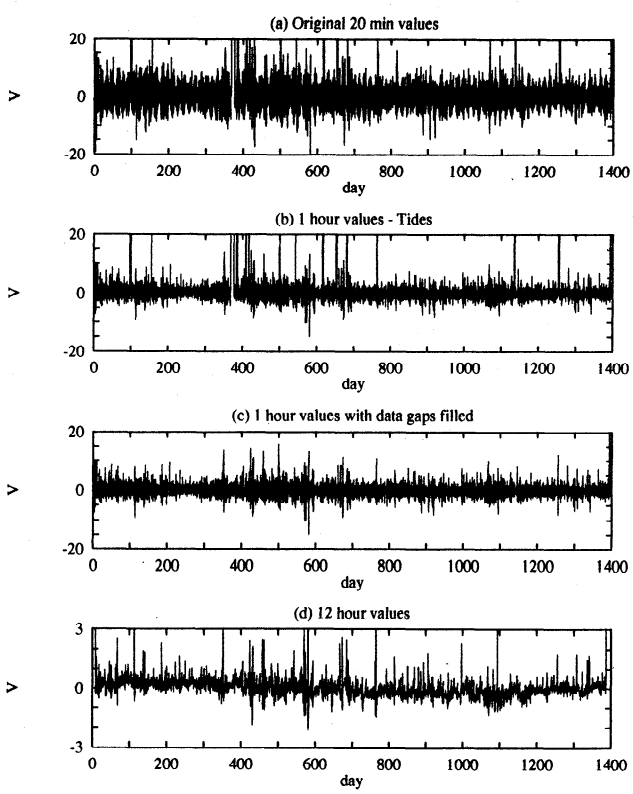

Figure 2. A 1400-day plot of the HAW-1 voltage from April 7, 1990, to March 2, 1994, showing (a) original 20 min median values, (b) 1 hour values with tides and solar daily variation removed, (c) 1 hour values with gaps filled as described in text, and (d) 12 hour values after decimation.

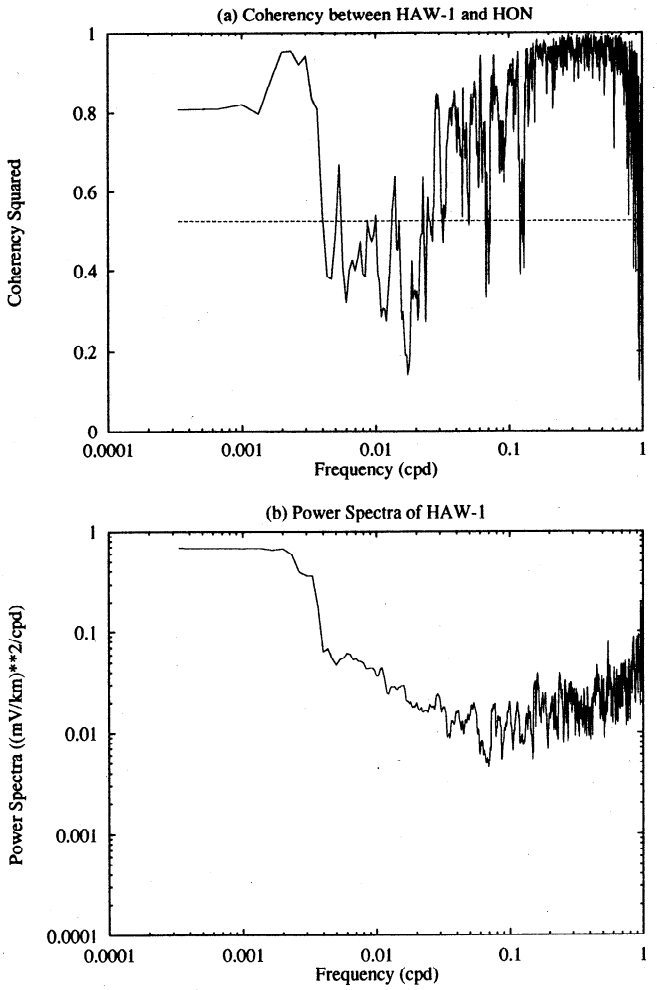

Figure 3. (a) Multiple squared coherence between the HAW-1 voltage and three components of the geomagnetic field at Honolulu (HON) for 1326 days. The dashed line is the zero-coherence level at 95% significance. The bandwidth of the estimate is 6.0×10^{-3} cpd. (b) Power spectrum of the HAW-1 voltage for the same 1326-day interval. The bandwidth of the estimate is 6.0×10^{-3} cpd.

gappy and reference data correlate with each other over periods corresponding to the gap duration.

Twelve hour values were then derived from the filled hourly mean time series after low-pass filtering. The 12-hour values in Figure 2d show large variations induced by geomagnetic storms. Indeed, the multiple squared coherence between the cable voltage and the three components of the geomagnetic field at HON suggests that the externally induced field is statistically significant in the cable voltage at frequencies higher than 3.7×10^{-2}cpd (periods less than 26 days) (Figure 3a). As discussed by *Chave et al.* [1992b], the externally induced field affects the cable voltage to a lower frequency than in electric field data from a point sensor because the small spatial scale components of the motionally induced voltage are filtered out by averaging over the long cable. However, power spectra of the cable voltage (Figure 3b) tend to increase with decreasing frequency to lower frequencies than was observed by *Chave et al.* [1992b]. This feature indicates that while motionally induced signals dominate at the lowest frequencies, separation of the motional signals from the external ones is necessary at intermediate to high ones.

4. Separation of Externally and Motionally Induced Field

An adaptive correlation cancellation filter developed by *Widrow and Stearns* [1985] was used to remove the externally induced voltage from the cable data. This algorithm calculates the time-varying impulse response function between the cable voltage and the three components of the geomagnetic field at HON using an least squares estimator and eliminates components of the cable voltage correlated with the latter, leaving only the motional component in the cable data. The only free parameters in the process are adaptation step size, scale factor of the step size, and filter length. The adaptation step size was selected automatically at each step based on the eigenvalues of the data correlation matrix based on a result given by *Widrow and Stearns* [1985]. The other free parameters were chosen empirically, but the results do not depend critically on their values.

The algorithm proceeds as follows. First, the mean and a linear trend were removed from all data sets, and an autoregressive (AR) filter was used to prewhiten the geomagnetic field at HON. The AR filter length was fixed at 1.5 days. The HAW-1 voltage is already nearly white and hence was not prewhitened. Second, the scale factor for the adaptation step size was tested from 10^{-5} to 0.1 for a given filter length, and the best value was selected on the basis of goodness of fit. This quantity

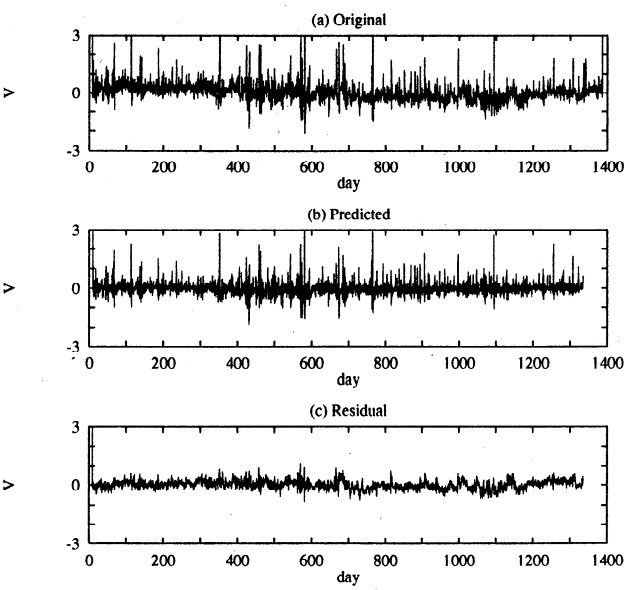

Figure 4. A 1400-day plot of the HAW-1 voltage from April 7, 1990, to March 2, 1994, showing the (a) original 12-hour values, (b) externally induced field predicted by adaptive filtering as described in text, and (c) motionally induced residuals from the filtering operation.

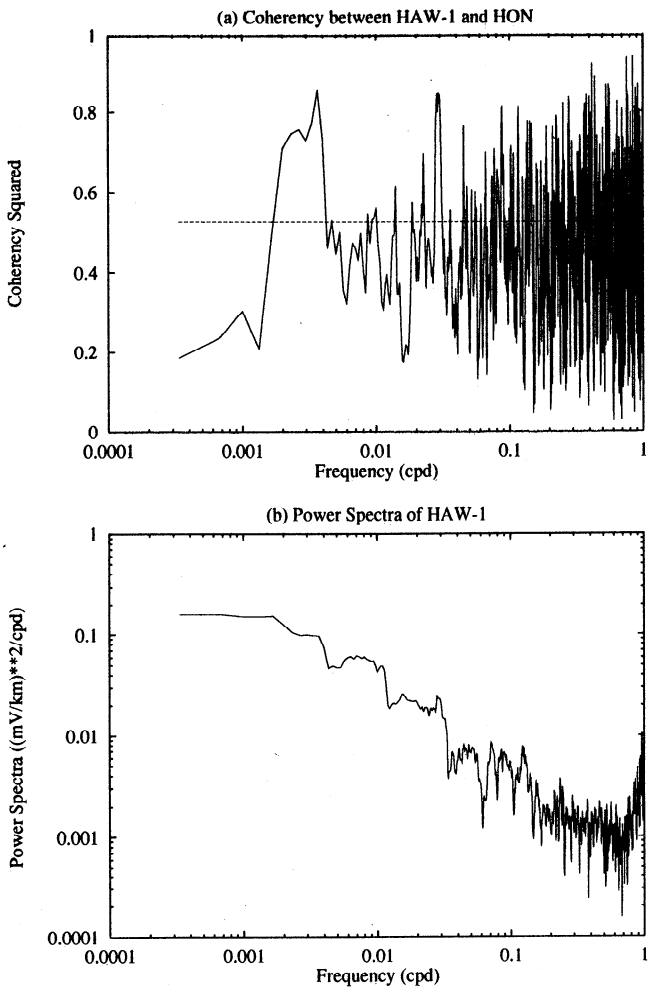

Figure 5. (a) Multiple squared coherence between the motionally induced cable voltage and three components of the geomagnetic field observed at HON. The dashed line is the zero coherence level at 95% significance. The bandwidth of the estimate is 6.0×10^{-3} cpd. (b) Power spectrum of the motionally induced field. The bandwidth of the estimate is 6.0×10^{-3} cpd, and there are 16 degrees of freedom, yielding an approximate 95% confidence level of (0.55, 2.32) times the estimates.

typically changes slowly with either scale factor or filter length. Third, the best filter length was determined by comparing time series, power spectra, and coherence of results for different filter lengths. The filters tested ranged from 6.5 to 26.5 days in length. The variance monotonically decreased with filter length. However, the rate of decrease became substantially slower for lengths beyond 22.5 days, and increases in filter length beyond this point affected only the highest frequencies, which are not of interest in this study. Thus a filter length of 22.5 days was selected.

The original and predicted cable voltages and the residual from the filtering operation are shown in Figure 4. Since the externally induced field is the major component in the predicted voltage, the motionally induced voltage is expected to be the dominant component in the residual. This can be verified visually by comparing

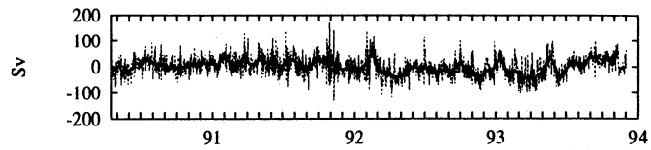

Figure 6. Approximate estimate of the transport from the motionally induced voltage (dashed line). The low-pass-filtered transport with a cutoff period at 25 days is also shown (solid line). The first day is April 16, 1990, and the time axis is marked at monthly intervals.

Figures 3 and 5. The squared coherence between the motionally induced voltage and the geomagnetic field at HON is much smaller than that without filtering at periods shorter than about 27 days (1 solar cycle). The power spectrum of the residual drops by 1 or 2 decades compared with that of the original over the same period band. These indicate that the filtering procedure

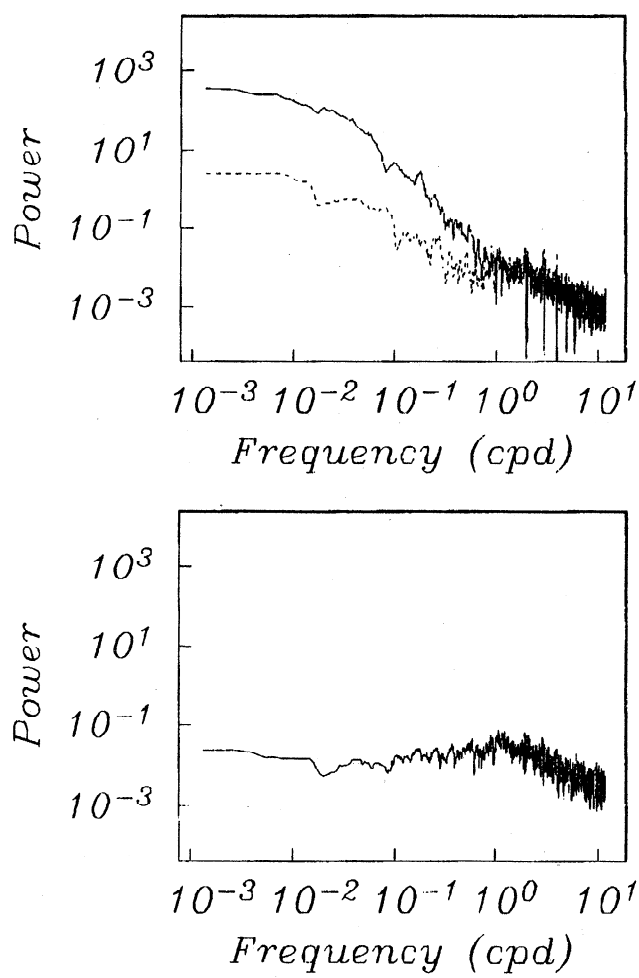

Figure 7. Comparison of the power spectrum (in mV^2/km^2 per cpd) of hourly means of (top) point sensors and (bottom) HAW-1 cable. Solid line in Figure 7, top, is from a site located beneath the Gulf Stream, while the dashed line is from a weak eddy variability region in the North Pacific. In Figure 7, bottom, the time interval April 1990 to April 1991 is used [from *Chave et al,* 1992b].

Table 1. Seasonal Variance of the Motionally Induced Voltage From 1990 to 1993

Season	1990	1991	1992	1993
Jan.-March		0.03563	0.07631	0.07380
April-June	0.02827	0.04401	0.03835	0.06819
July-Sept.	0.02836	0.04688	0.02475	0.02421
Oct.-Dec.	0.02504	0.05977	0.04962	0.03112

Values are in V^2.

of Figure 4 has been effective in removing geomagnetic noise.

The motionally induced field may be approximately converted into the transport in Figure 6, assuming that the dimensionless scale factor C, geomagnetic field F_z, and water depth D are 1.0, 26356.6 nT, and 4000 m, respectively. The scale factor is set at the maximum possible value, while the other two are rough averages over the cable length. The low-pass-filtered transport with the cutoff period at 25 days is also shown. The amplitude is rather small, indicating that spatial averaging has had a major effect. This is further supported by comparison of the power spectra for a point sensor and the cable (Figure 7).

Seasonal variations in the cable voltage are apparent, as are longer-term ones. The seasonal variance is listed in Table 1. The variance is largest in winter (January to March), which is consistent with the known features of the wind field. Interannual changes in the variance are also apparent.

5. Comparison With Atmospheric Variables

5.1. Wind Stress Curl

The motionally induced voltage cannot be precisely transformed to mass transport because there are no independent transport measurements along the cable to calibrate the dimensionless scale factor C in (1) and account for its lateral variations. Therefore the features of the motionally induced voltage will be investigated indirectly.

Chave et al. [1992b] noted that the first year of the HAW-1 cable data set showed significant coherence with the vertical component of the wind stress curl (hereinafter referred to as curl) in the North Pacific. Curl provides the primary forcing for wind-driven barotropic flow at subinertial frequencies through the linear response of an ocean to atmospheric forcing [*Philander*, 1978]. This phenomenon is well understood as the transmission of vorticity from the wind to the ocean through Ekman pumping.

Atmospheric forcing dominates the variability of large-scale barotropic flows in regions far from energetic western boundary currents at periods less than about 100 days. The wind-driven flow has previously been detected by demonstrating significant two-point coherence between the atmospheric variables (either wind stress, curl, or surface air pressure) and barotropic flow proxies (either water velocity, induced voltage, or pressure fluctuations at the ocean bottom) [e.g., *Dickson et al.*, 1982; *Koblinsky and Niiler*, 1982; *Niiler and Koblinsky*, 1985; *Brink*, 1989; *Luther et al.*, 1990; *Samelson*, 1990; *Cummins and Freeland*, 1993; *Chave et al.*, 1992a]. A number of model studies based on linear, viscid, quasi-geostrophic dynamics with stochastic atmospheric forcing have also been carried out to predict or support these observations [e.g., *Frankignoul and Müller*, 1979; *Willebrand et al.*, 1980; *Müller and Frankignoul*, 1981; *Brink*, 1989; *Samelson*, 1989; *Samelson and Shrayer*, 1991; *Cummins*, 1991; *Lippert and Müller*, 1995; *Brink and Samelson*, 1998].

Thus the motionally induced component of the HAW-1 voltage is expected to reflect wind-driven barotropic flows in the eastern Pacific at periods longer than several days, if a water transport phenomenon whose spatial scale is comparable to the cable length exists in the region. To investigate this hypothesis, we used the procedures developed by *Chave et al.* [1992a], in which spatial maps of the coherence between the cable voltage and atmospheric variables were constructed as a function of period, and maps of the intercorrelation between the atmospheric variables themselves are used to remove ambiguities.

5.2. Coherence Maps

The wind velocity at 10 m height and surface air pressure were provided by the European Centre for Medium-Range Weather Forecasts (ECMWF). The ECMWF products consist of assimilated 12-hour values for 3933 sites spaced every 2.5° over the entire Pacific. The wind stress was computed from the wind velocity as in the work by *Chave et al.* [1991], and then the vertical component of the wind stress curl was obtained at 3685 points from the wind stress at nine adjacent points using a two-dimensional finite difference formula in spherical coordinates, as described by *Chave et al.* [1991]. Consistency of the ECMWF product with the Fleet Numerical Oceanigraphy Center (FNOC) product (which was used by *Luther et al.* [1990] and *Chave et al.* [1992a, b]) has previously been verified [e.g., *Chave et al.*, 1991, and references therein]. The spatial distribution of the ECMWF product is more sparse than that of the FNOC product, and therefore the ECMWF wind field is expected to lack some short-scale components that may be present in the FNOC result. For example, *Liu et al.* [1998] reported that the ECMWF product missed short-wavelength features at coastal and equatorial points in comparison with scatterometer satellite observations. However, the cable will mainly reflect large-scale barotropic flow and hence deficiencies of the ECMWF product as a reference are not expected to be a limitation.

Table 2. Calculated Periods With Both Sides Limits for the 3.6-Year Segment

Period,days	Lower Limit	Upper Limit
221.00	147.33	442.00
132.60	102.00	189.43
94.71	78.00	120.55
73.67	63.14	88.40
60.27	53.04	69.79
51.00	45.72	57.65
44.20	40.18	49.11
39.00	35.84	42.77
34.89	32.34	37.89
31.57	29.47	34.00
28.83	27.06	30.84
26.52	25.02	28.21
24.56	23.26	26.00
22.86	21.74	24.11
21.39	20.40	22.47
20.09	19.22	21.05
18.94	18.16	19.79
17.92	17.22	18.68
17.00	16.37	17.68
16.17	15.60	16.78
15.42	14.90	15.98
14.73	14.26	15.24
14.11	13.67	14.57
13.53	13.13	13.96
13.00	12.63	13.39
12.51	12.17	12.87
12.05	11.73	12.39
11.63	11.33	11.95
11.24	10.96	11.53
10.87	10.61	11.14
10.52	10.28	10.78
10.20	9.97	10.44
9.90	9.68	10.12
9.61	9.40	9.82
9.34	9.14	9.54
9.08	8.90	9.27
8.84	8.67	9.02
8.61	8.45	8.78
8.39	8.24	8.55
8.19	8.04	8.34
7.99	7.85	8.13
7.80	7.66	7.94
7.62	7.49	7.75
7.45	7.33	7.58
7.29	7.17	7.41
7.13	7.02	7.25
6.98	6.87	7.09
6.84	6.73	6.94
6.70	6.60	6.80
6.56	6.47	6.66
6.44	6.34	6.53
6.31	6.23	6.41
6.20	6.11	6.28
6.08	6.00	6.17
5.97	5.89	6.05
5.87	5.79	5.95
5.77	5.69	5.84
5.67	5.59	5.74
5.57	5.50	5.64
5.48	5.41	5.55
5.39	5.33	5.46
5.30	5.24	5.37
5.22	5.16	5.28
5.14	5.08	5.20
5.06	5.00	5.12

The squared coherence between the cable voltage and an atmospheric variable at each of the 3933 grid points (3685 for the curl) was computed as a function of period. The atmospheric variables used were the curl, meridional and zonal wind stresses, and surface pressure, following *Brink* [1989], *Luther et al.* [1990], and *Chave et al.* [1992a]. Except for curl, these variables do not have a direct forcing relationship with the cable voltage, but they do show significant coherence. This is because the wind stress and surface pressure are coherent with curl and, consequently, can serve as proxies for it. They actually played important roles in the work by *Chave et al.* [1992a] in detecting the influence of intercorrelation of the atmospheric variables and hence elucidating the correct forcing relation between curl and barotropic velocity.

Sixty-five periods for the entire 3.6-year data set and 18 for the individual years were selected with upper and lower limits as listed in Tables 2 and 3, respectively. In a free wave regime, the wavenumber bandwidth and frequency bandwidth are directly proportional, and hence wide frequency bandwidths can result in reduced coherence due to decorrelation. As a consequence, the time-bandwidth product (TBW) was fixed at the low value of 4 for all calculations. All spectral estimates were computed using the multiple-window method of *Thomson* [1982], and hence the approximate degrees of

Table 3. Calculated Periods With Both Sides Limits for the Each Year Segment

Period,days	Lower Limit	Upper Limit
60.83	40.56	121.67
36.50	28.08	52.14
26.07	21.47	33.18
20.28	17.38	24.33
16.59	14.60	19.21
14.04	12.59	15.87
12.17	11.06	13.52
10.74	9.86	11.77
9.61	8.90	10.43
8.69	8.11	9.36
7.93	7.45	8.49
7.30	6.89	7.77
6.76	6.40	7.16
6.29	5.98	6.64
5.89	5.62	6.19
5.53	5.29	5.79
5.21	5.00	5.45
4.93	4.74	5.14

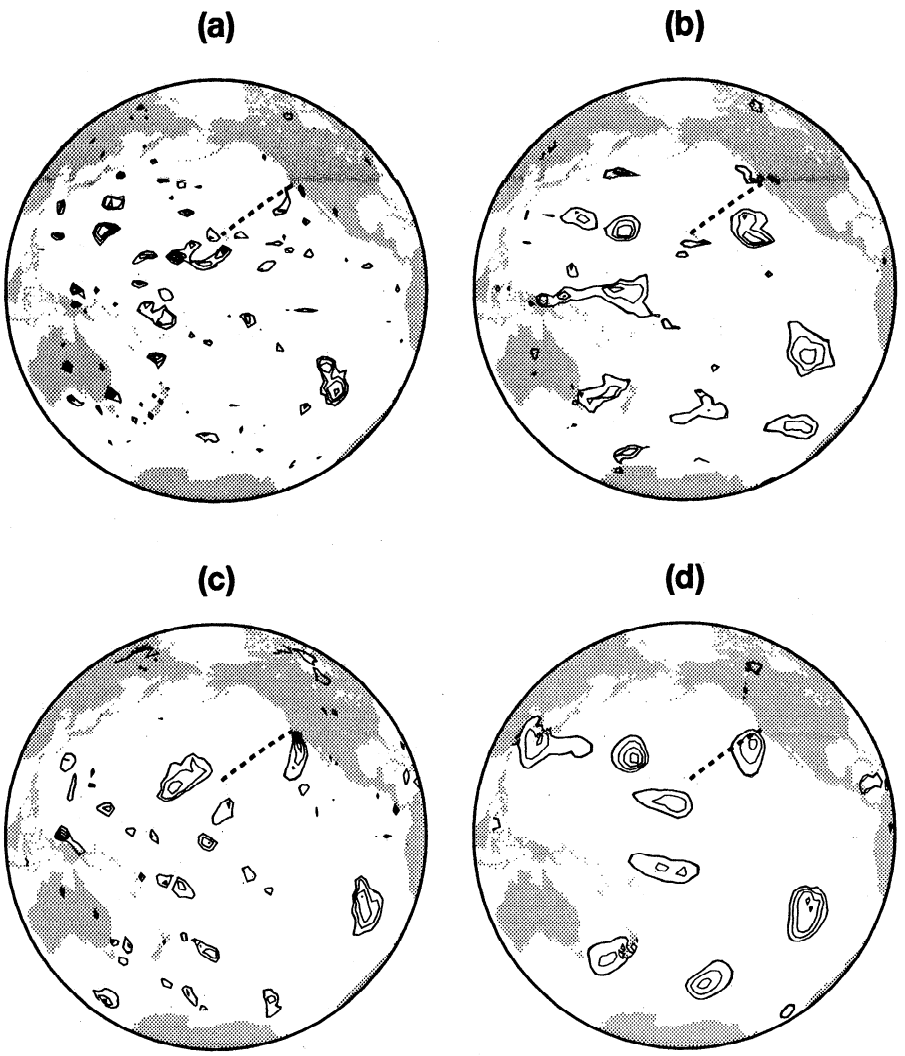

Figure 8. Coherence maps between the 3.6-year-long cable voltage time series and (a) curl, (b) zonal wind stress, (c) meridional wind stress, and (d) surface pressure at 32 days. Only values of the squared coherence larger than 0.39 (which is the zero-coherence level at 95% significance) are contoured. The contour interval is 0.1 from 0.4 to 1.0.

freedom is twice the number of orthogonal tapers used in the estimate [2 × (2 × TBW -1) in this instance]. Assuming Gaussian data, this yields a zero-coherence level at 95% significance of 0.39 for two-point coherences.

Contour maps between the cable voltage and atmospheric variables over the Pacific basin were produced for significantly coherent points ($\geq$ 0.39) at each period. Figures 8a-8d are coherence maps at a period of 32 days between the cable voltage and curl, zonal, and meridional wind stresses and surface pressure, respectively. Typical features of the maps at all periods are seen in Figure 8 as follows: (1) significant local and nonlocal coherence patches are seen between the cable voltage and all atmospheric variables; (2) coherent patches of various sizes are scattered over the region for curl, while these tend to have the largest sizes for pressure and intermediate values for wind stress; and (3) the peak values are highest in maps of the curl. These features are consistent with the results of *Chave et al.* [1992a, b]. These further indicate that there exists a large-scale component of the wind-driven ocean current that is not diminished by integration over the horizontal scale of the cable and hence that the cable works well as a barotropic current meter.

However, it should be noted that some of the nonlocal coherence reflects intercoherence of curl rather than direct atmospheric forcing. The curl field is known to show significant spatial coherence with itself or teleconnections [e.g., *Chave et al.*, 1991]. This can produce false coherent patches in the curl-voltage coherence, which must be detected and removed.

5.3. Selection

Chave et al. [1992a] proposed an empirical procedure to detect coherence patches due to teleconnection. It consists of three steps. First, coherence max-

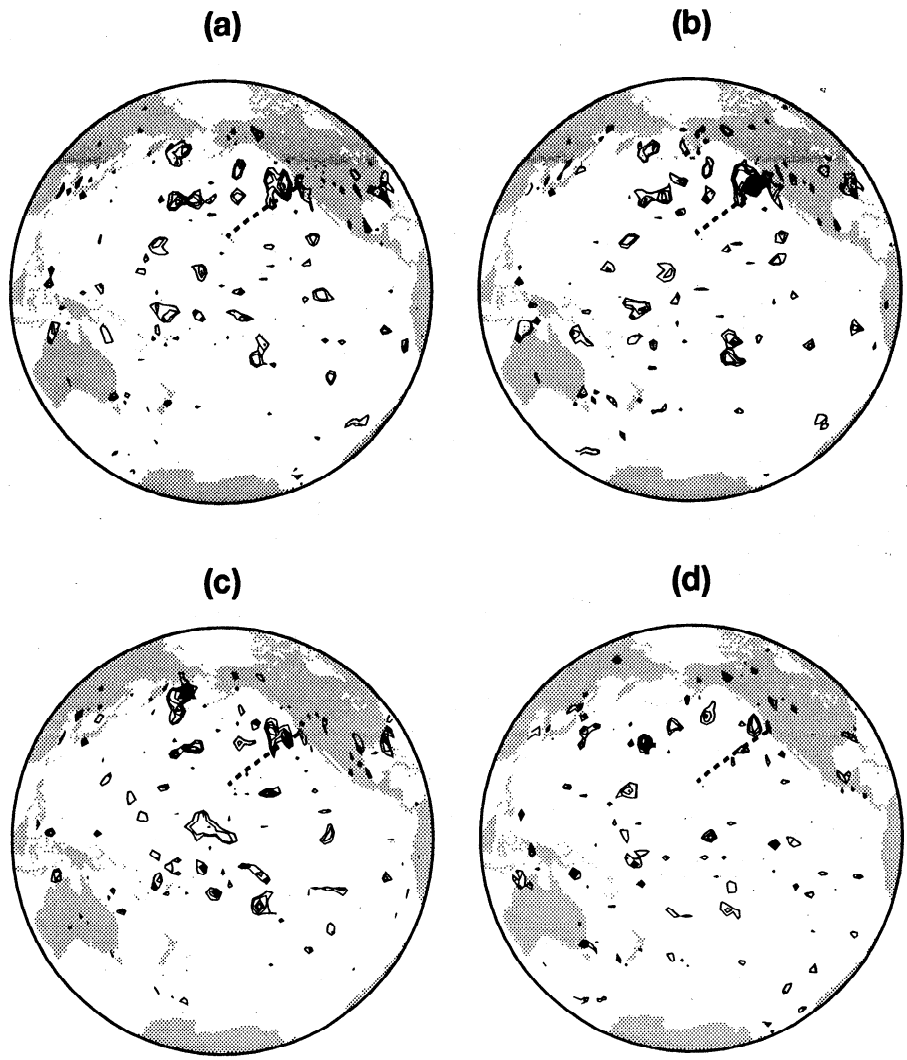

Figure 9. Comparison of the original coherence and intercoherence maps of curl, showing (a) the coherence between the curl at all points and the cable voltage and intercoherence maps between the curl at (b) candidate site 1 (solid circle), (c) candidate site 2 (solid triangle), and (d) candidate site 3 (cross) with curl at all remaining locations at a period of 7 days. Contouring details are the same as in Figure 8.

ima between cable voltage and curl are chosen from those patches that include more than a few grid points (roughly 1000 km or more in scale). We chose only the maxima from large patches because there is always the possibility that statistical variability will cause some points to exceed the zero-coherence level at 95% significance, and hence it is dangerous to trust high coherence at isolated points. It is far less likely that this will occur simultaneously over large areas and especially at subadjacent points where intercorrelation of the ECMWF product is weak. Second, intercoherence between curl at a selected point and an atmospheric variable (either curl, meridional or zonal wind stress, or surface pressure) at each of the remaining grid points is computed and is contoured into an intercoherence map. Figures 9-12 are the intercoherence coherence maps at a 7-day period in which there are three candidate points marked with a solid circle, triangle, and cross. Third, the intercoherence maps are compared with the original ones and a curl that can reproduce the original maps is determined. For example, maps of candidates 1 (Figure 9b) and 2 (Figure 9c) reasonably reproduce the original voltage-curl coherence map (Figure 9a), but the map of candidate 3 (Figure 9d) does not. Then, from Figures 10a-10c it can be concluded that the intercoherence map of candidate 1 is more similar to the original voltage-pressure map than that of candidate 2. The intercorrelation maps between the curl and wind stress also support this tendency (Figures 11 and 12). Comparison of pressure maps is generally more effective than for wind stress. Maps of candidate 3 do not resemble the original in all atmospheric variables (Figures 9-12). Therefore curl at candidate 1 is considered to be the most similar to the voltage, and the patches that con-

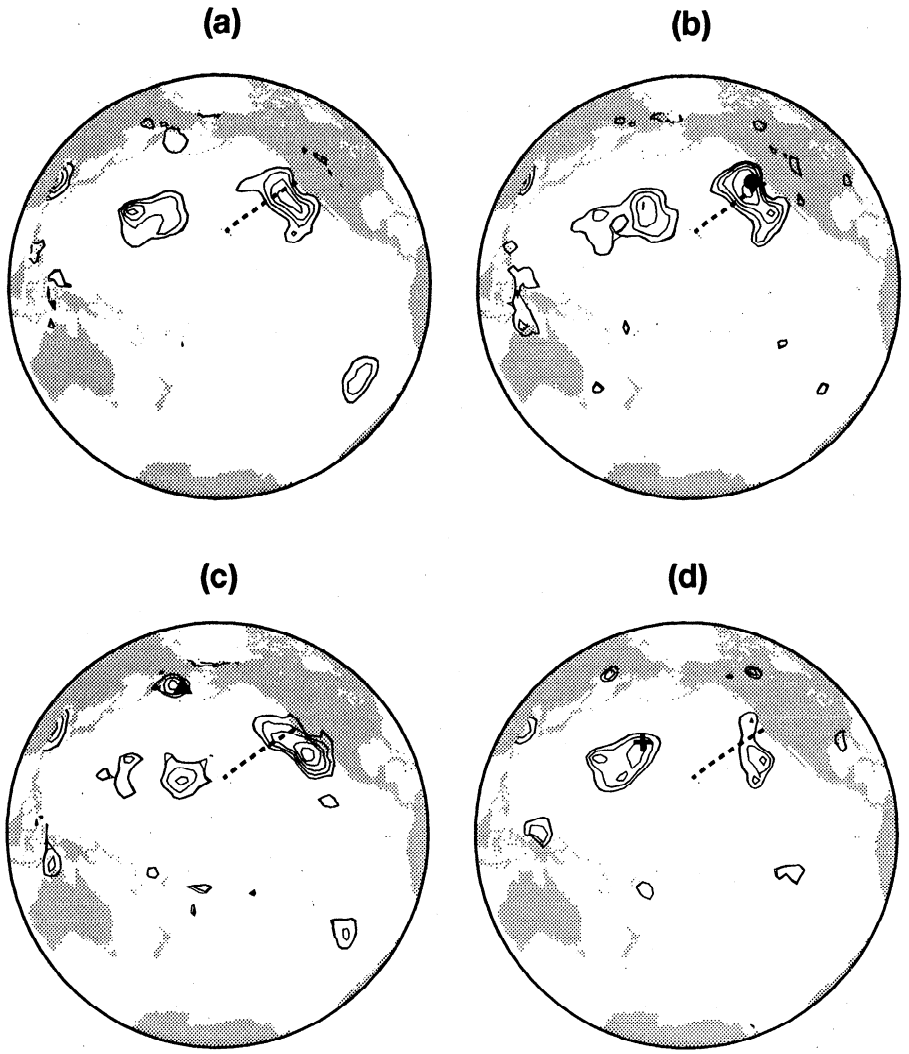

Figure 10. Comparison of the original coherence and intercoherence maps of air pressure, showing (a) coherence between surface air pressure at all sites and cable voltage and intercoherence maps between curl at (b) candidate site 1 (solid circle), (c) candidate site 2 (solid triangle), and (d) candidate site 3 (cross) with air pressure at all remaining locatioons at a period of 7 days. Contouring details are the same as in Figure 8.

tain candidates 2 and 3 are ruled out because their similarity to the voltage is less clear and hence they probably reflect teleconnection. The principal idea behind this procedure is that curl will be most coherent with the cable voltage when it is connected with curl through atmospheric forcing rather than indirectly through teleconnection.

This procedure is subjective, and there is no mathematical guarantee that it will work. Nevertheless, it was shown to be successful by *Chave et al.* [1992a], who demonstrated consistency of the location of the inferred curl forcing region with the propagation direction estimated from multiple coherent sensors. Since there is no other independent observation of large-scale water transport along the HAW-1 cable, this pattern-matching procedure was applied to the present cable data set to detect and eliminate coherent patches that are produced by the teleconnection. A total of 369 coherence maxima at 35 periods were examined for the 3.6-year segment, and 1476 intercoherence maps were produced in total. There were 336 patches judged to be produced by teleconnection of the curl field, and 33 patches remained at 21 periods.

5.4. Results

The 21 selected center periods were divided into six period bands: 5.1-5.6, 5.7-9.9, 11.2-14.7, 17-20, 32-44, and 95-133 days. Although *Chave et al.* [1992b] reported that no significant coherence appeared at periods shorter than 20 days in the analysis of the first-year data set, the present procedure to remove geomagnetic noise substantially improved the data quality and made analysis at shorter periods possible in this study. Owing to the much longer record, the period bands of the

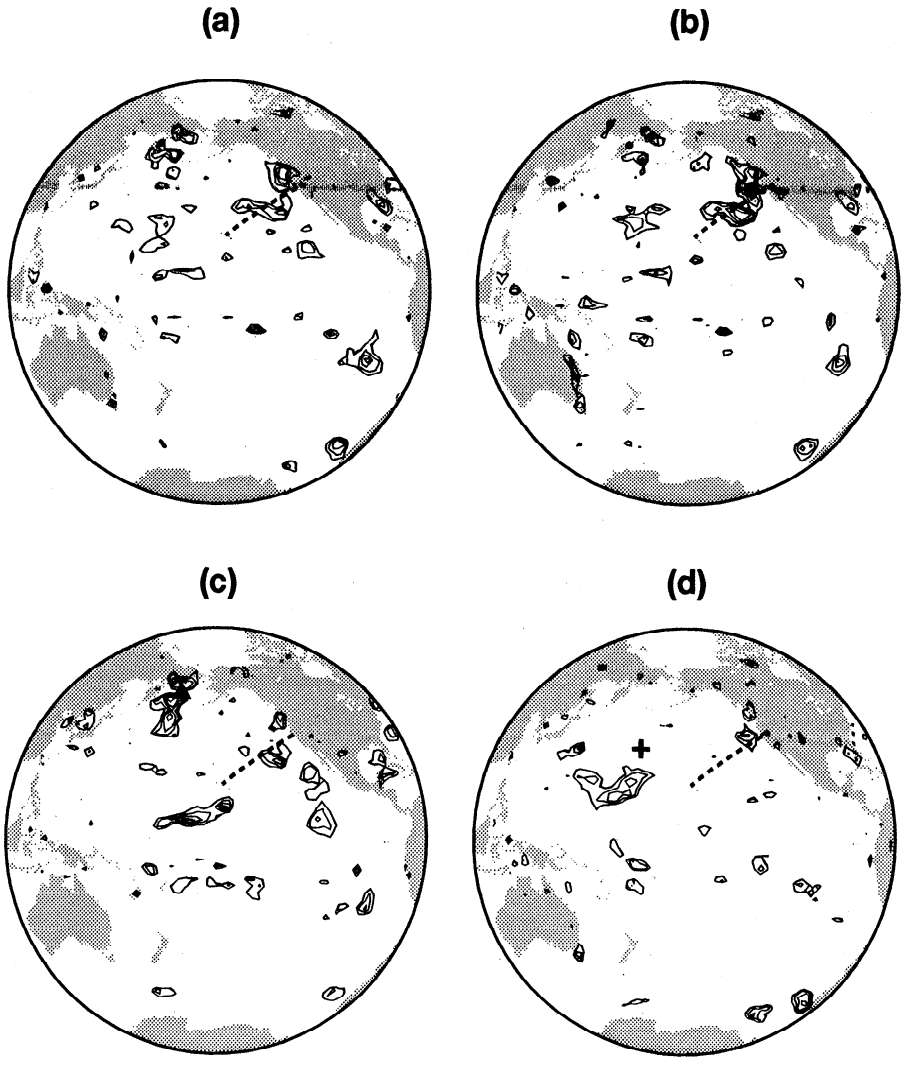

Figure 11. Comparison of the original coherence and intercoherence maps of zonal wind stress, showing (a) coherence between the zonal wind stress at all sites and the cable voltage and intercoherence maps between curl at (b) candidate site 1 (solid circle), (c) candidate site 2 (solid triangle), and (d) candidate site 3 (cross) with zonal wind stress at all remaining sites at a period of 7 days. Contouring details are the same as for Figure 8.

barotropic currents are more finely resolved than those observed by *Brink* [1989] (3.7-8, 8-23, and 23-76 days) and *Chave et al.* [1992a] (6-8, 10-14, and 20-50 days). Each period band also corresponds to the location of minor power spectral peaks in the cable voltage as shown in Figure 13.

Examples of the voltage-curl coherence maps are shown in Figure 14. The selected coherence maxima are marked by solid triangles. Coherence maxima of the selected patches are typically 0.6-0.8, and their diameters are of the order of 1000 km. Values of the coherence at the maxima are as high as those for a point sensor [*Chave et al.*, 1992a] and much higher than those for a moored current meter [*Brink*, 1989]. Spatial scales of the patches are larger or at least comparable with results from those studies.

The spatial patterns of coherence vary considerably with period, indicating complexity of the wavenumber structure in the wind-driven flow field. Coherence patches spread over various parts of the Pacific basin. There is no particular tendency for the pattern to change with period. The maxima are local at some period bands (95, 19, and 7 days) and nonlocal at others (44 and 13 days) in Figure 14. The spatial patterns are often very complicated, even within a given period band. Significant coherence is seen in equatorial regions only in the 1.2- to 14.7-day band. Patterns change especially quickly with period in the shortest two bands.

A new feature of this study is the very large separation of the nonlocal maxima (up to 10,000 km) from the cable. For example, maxima are seen in the southeast Pacific (20°-50°S, 80°-120°W) at 44 and 32 days

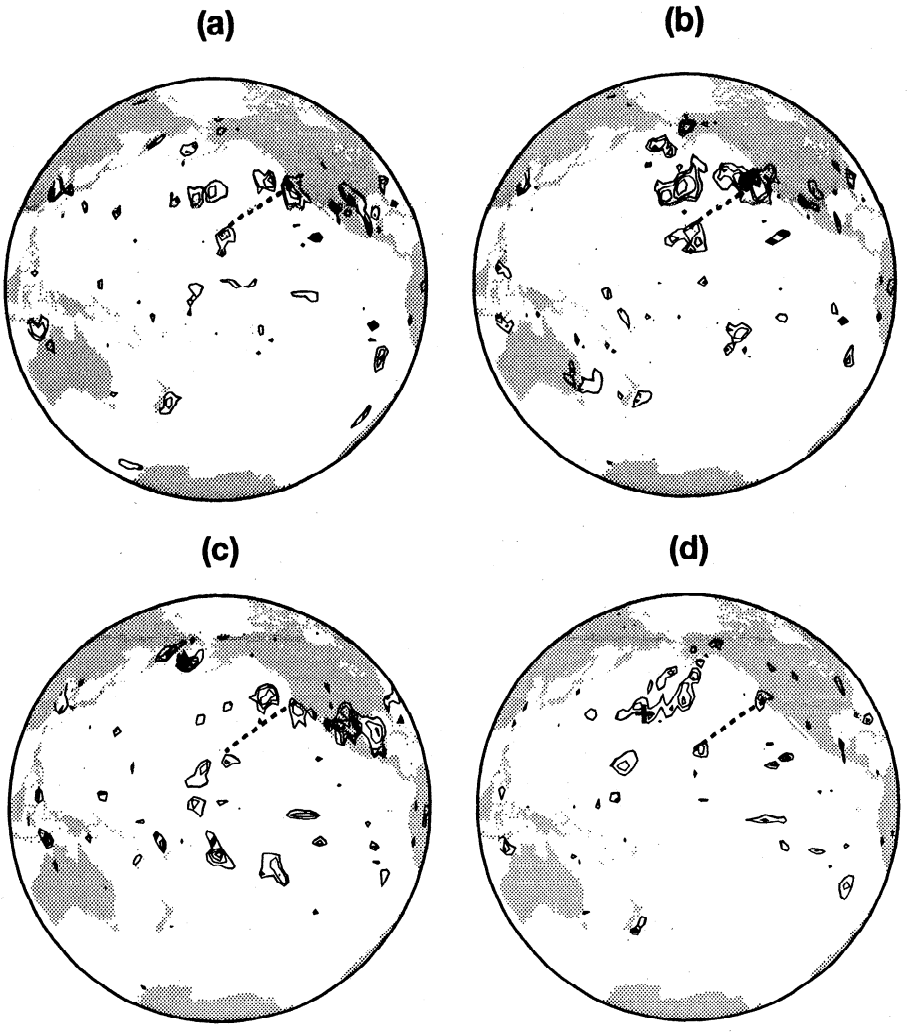

Figure 12. Comparison of the original coherence and intercoherence maps of meridional wind stress, showing (a) coherence between the meridional wind stress at all sites and the cable voltage and intercoherence maps between curl at (b) candidate site 1 (solid circle), (c) candidate site 2 (solid triangle), and (d) candidate site 3 (cross) with meridional wind stress at a period of 7 days. Contouring details are the same as for Figure 8.

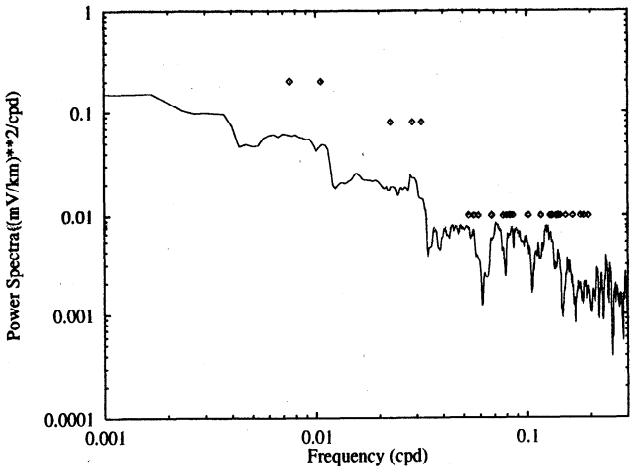

Figure 13. Frequencies where significant forcing relations between cable voltage and atmospheric variables are detected (diamonds) superimposed on a power spectrum of the cable voltage (solid line).

in the 32- to 44-day band, and coherence maps with all atmospheric variables show significant coherent patches nearby. In the 11.2- to 14.7-day band, the selected maxima are in the equatorial region (100°-130°W for 13 days, 150° E-140°W for 12.5, 12, and 11.6 days) and occasionally in the Tasman Sea (13 and 12 days).

Temporal variation in the wind-driven velocity is seen in the power spectra in Figure 15, which compares spectra for each year (beginning in mid-April). For example, the power spectral level at 30-40 days increases year by year, but that at 6-9 days remains at almost the same level. Since power spectral peaks correspond to significant coherence patches for the 3.6-year segment, temporal variations of the coherence between the oceanic and atmospheric variables are expected. Figure 16 shows coherence maps between the voltage and curl at 39 days for 3.6 years and at 37 days for each year. The map of the third year shows much larger coherent patches than those of the other years, as expected from the differ-

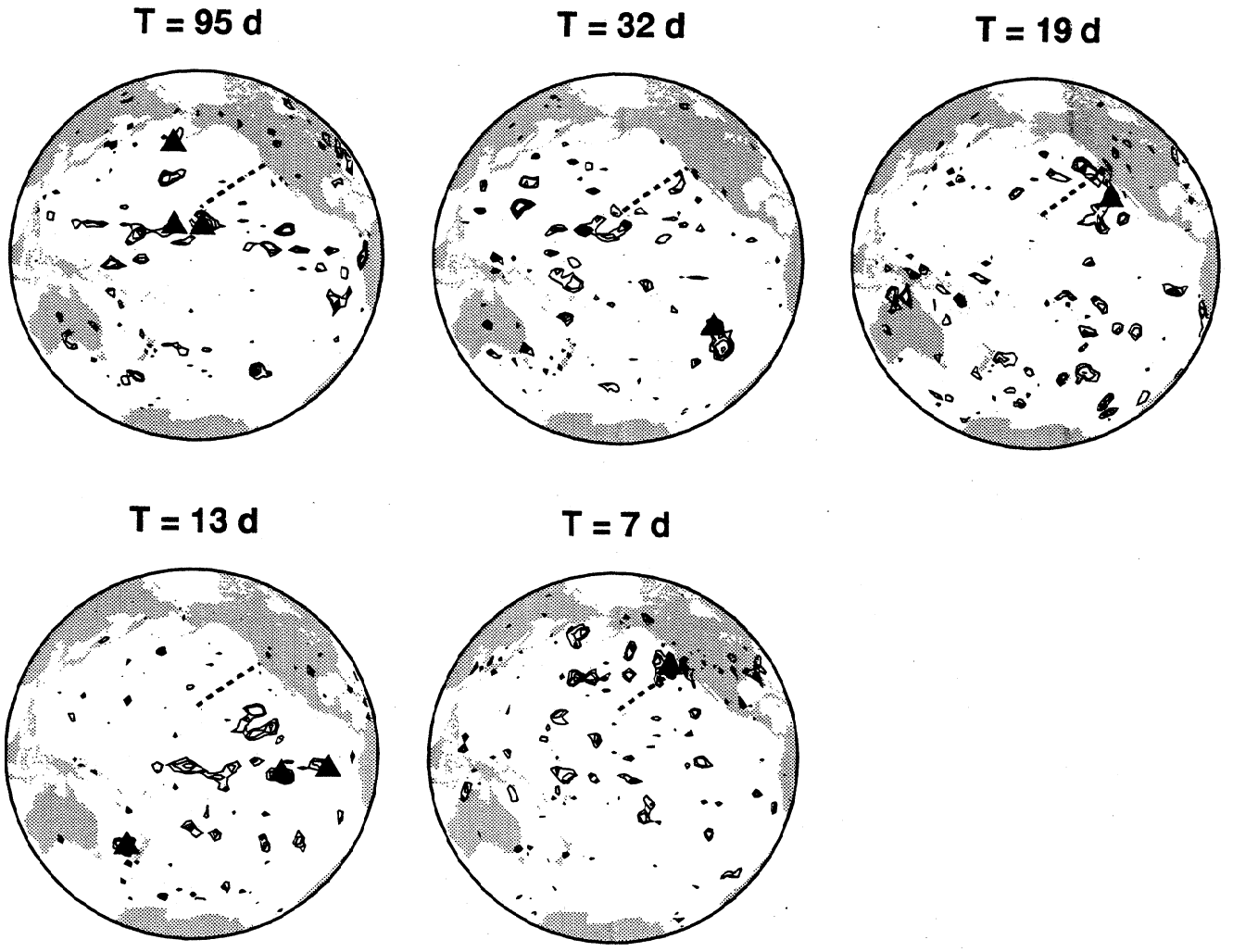

Figure 14. Coherence maps between the cable voltage and curl at 95, 32, 19, 13, and 7 days. The solid triangle indicates the preferred coherence maximum. Contouring details are the same as for Figure 8. The phases at the preferred maxima with the solid triangle at 95 days are -155°, -145°, and -163° counterclockwise from the northernmost maximum. Those at 32, 19, and 7 days are -134°, 167°, and 41°, respectively. Those at 13 days from the western to eastern maxima are 52°, 177°, and -68°, respectively. A positive phase value means that the curl leads the cable voltage.

ences in power. The map of the 3.6-year segment looks like an intermediate value for the 3 years, but the influence of the third year is greater than the other two. In the period band at 6-9 days, high activity can be found for all segments of the data (not shown here). These tendencies are supported by coherence maps between the voltage and other atmospheric variables. Figure 17 shows the voltage-pressure coherence maps for the same data segments as Figures 16. The voltage-pressure coherence at 37 days for the third year shows a patch with a striking spatial scale ($> 10,000$ km) and high maximum coherence (0.7-0.9).

6. Discussion

The motionally induced voltage on the cable shows many similarities to those from a point sensor. This fact encourages further studies of the large-scale barotropic flows using basin- to planetary-scale submarine cables. Since the flow patterns are extremely complicated as shown in this study, observation and comparison with multiple sensors are essential. The network of submarine cables in the Pacific which currently is being monitored will be an ideal tool to assess this subject (Figure 18). For example, flow directions might be detectable through networked observations and will contribute to interpretation of coherence maxima.

In the study of *Chave et al.* [1992a], the coherence between curl and barotropic velocity observed by an ocean bottom electrometer was consistently larger than that for moored current meters, largely because baroclinic noise was effectively eliminated by the inherent vertical averaging in $\langle \mathbf{v}_h \rangle^*$. This is also the case for the cable voltage, as its coherence peaks are 0.6-0.8. However, horizontal averaging along the cable decreases the

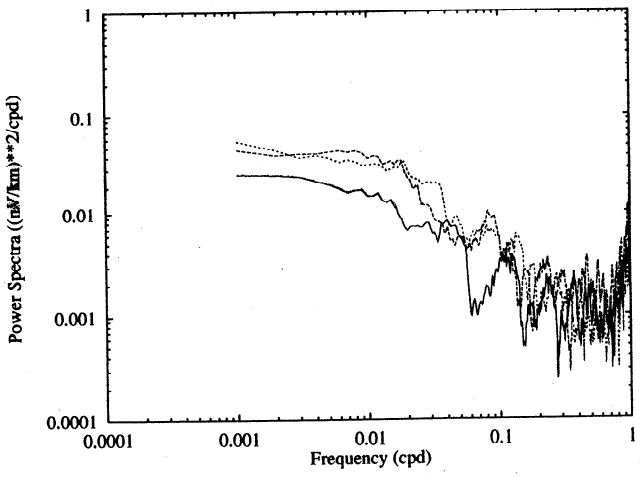

Figure 15. Power spectra of yearlong time series of cable voltage beginning April 1990 (solid line), April 1991 (dashed line), and April 1992 (dotted line). The bandwidth of the estimates are 6.0×10^{-3} cpd, and there are 16 degrees of freedom, yielding an approximate 95% confidence level of (0.55, 2.32) times the estimates.

amplitude of the motionally induced field, and consequently, the geomagnetic noise is more severe at periods shorter than 27 days unless removed. However, the coherence between the HAW-1 voltage and the geomagnetic field at HON is consistently low at periods up to about 1 year. The use of cable voltages from periods of 27 days to 1 year may be more effective in terms of the signal-to-noise ratio, even if the externally induced voltage is only crudely removed. That period band contains the so-called resonant regime and the Sverdrup regime according to a number of model studies. In the resonant regime at periods from a few to about 100 days, the ocean response is barotropic and can be nonlocal because freely propagating Rossby waves tend to be excited. Periods longer than 100 days lie in the Sverdrup regime, where a Sverdrup balance is expected and hence the response should be local. These assertions must be modified owing to the influence of topography and can be tested using cable data. Further, since a long-term data set is available in the case of submarine cables, the frequency bandwidths can be narrow enough to prevent

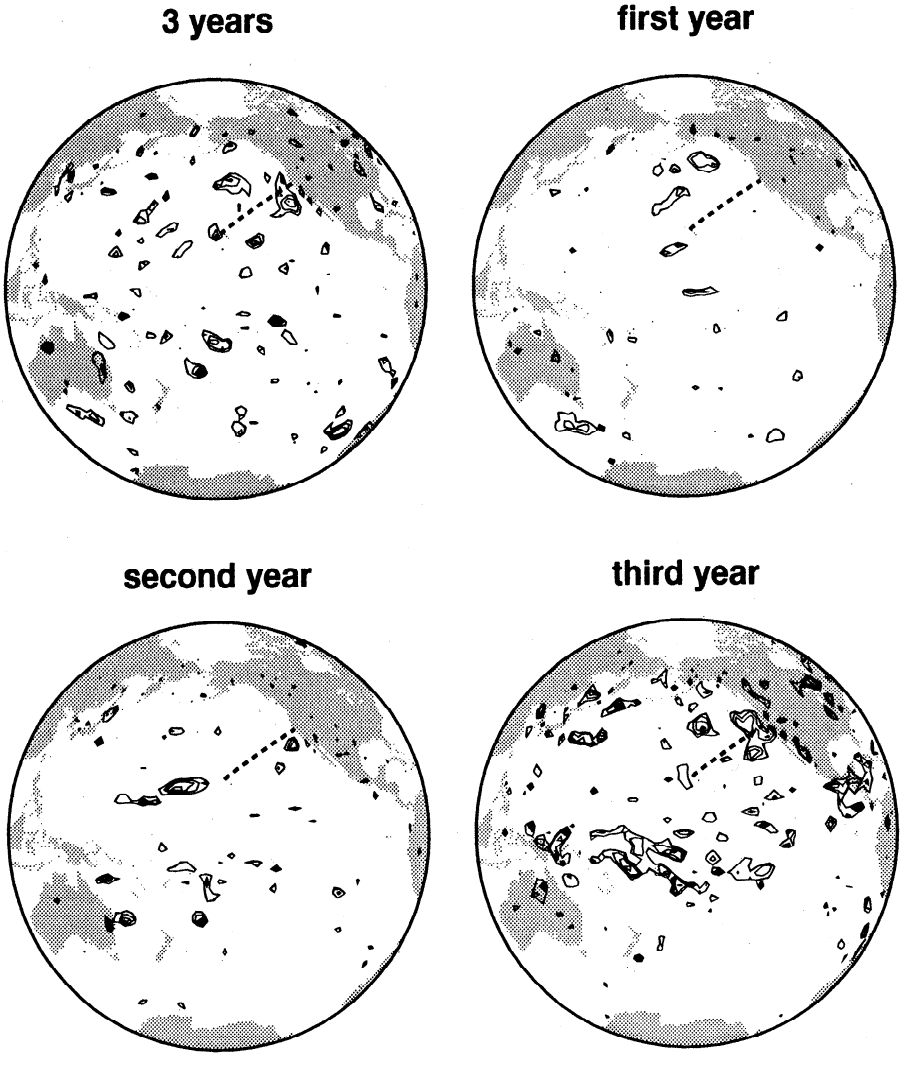

Figure 16. Coherence maps between the cable voltage and curl at 39 days (labeled 3 years) for 3.6 years and at 37 days for the first, second and third years. Contouring details are the same as for Figure 8.

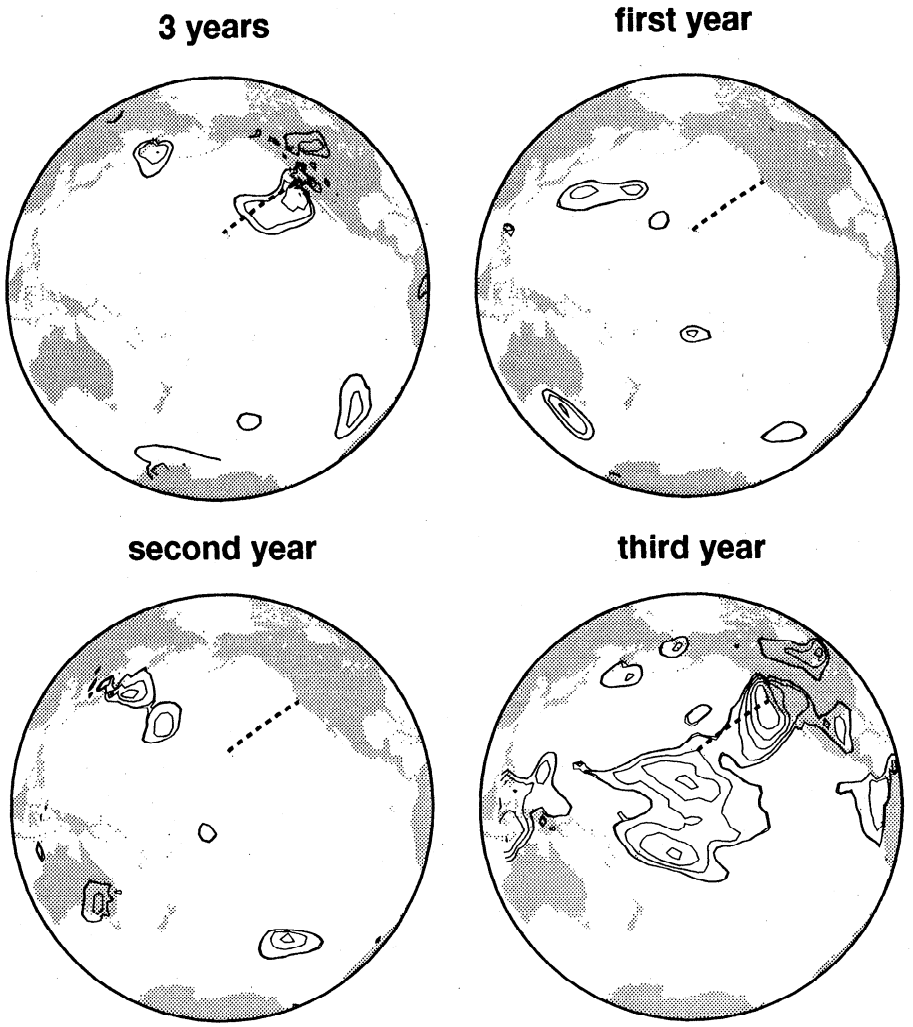

Figure 17. Coherence maps between the cable voltage and surface air pressure at 39 days (labeled 3 years) for 3.6 years and at 37 days for first, second and third years. Contouring details are the same as for Figure 8.

decorrelation from too large a wavenumber bandwidth. The cable network offers the possibility of resolving details of those two regimes and their transition zone.

7. Conclusion

The motionally induced field was extracted from a 3.6-year segment of the unpowered voltage observed on the HAW-1 cable. Amplitudes of the extracted voltage were rather small owing to spatial averaging of the motionally induced field. The extracted voltage has proven to be related to atmospheric variables (wind stress curl, wind stress, and surface pressure) computed from the ECMWF product. Significant coherence between the voltage and atmospheric variables was obtained at periods from 5-133 days over the entire Pacific basin. This indicates that the voltage was induced by large-scale, wind-driven barotropic flows in the region. Features of the wind-driven flows have proven to be complex, with both local and nonlocal coherence and coherence patterns that are highly variable in space and time. This probably reflects the complexity of the real wind field. An existing cable network that continuously records the voltages in various parts of the Pacific offers the long-term possibility of contributing to improvements in the interpretation of the wind-driven barotropic current.

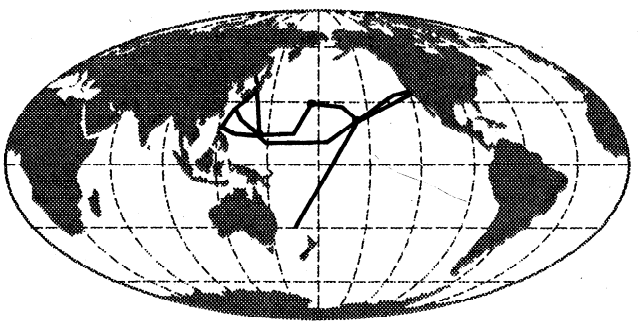

Figure 18. Submarine cable network in the Pacific that is being monitored at present.

Acknowledgments. We thank AT&T for providing access to the HAW-1 cable and hence making this study possible. We also thank L.J. Lanzerotti of Bell Labs for his assistance in providing access to the data. This work

was supported at WHOI by NSF grant OCE-9303890. This is WHOI contribution 9799 and Cambridge University Department of Earth Sciences and Institute of Theoretical Geophysics contribution 5363.

References

Bloom, G. L., Water transport and temperature measurements in the eastern Bering Strait, 1953-1958, *J. Geophys. Res., 69*, 3335-3353, 1964.

Brink, K.H., Evidence for wind-driven current fluctuations in the western North Atlantic, *J. Geophys. Res., 94*, 2029-2044, 1989.

Brink, K. H., and R. M. Samelson, Comments on "Direct atmospheric forcing of geostrophic eddies. Part II: Coherence Map", *J. Phys. Oceanogr., 28*, 1003-1009, 1998.

Chave, A. D., and D. S. Luther, Low frequency, motionally induced electromagnetic fields in the ocean, 1, Theory, *J. Geophys. Res., 95*, 7185-7200, 1990.

Chave, A. D., D. S. Luther, and J. H. Filloux, Variability of the wind stress curl over the north Pacific: Implications for the oceanic response, *J. Geophys. Res., 96*, 18,361-18,379, 1991.

Chave, A. D., D. S. Luther, and J. H. Filloux, The barotropic electromagnetic and pressure experiment, 1, Barotropic current response to atmospheric forcing, *J. Geophys. Res., 97*, 9565-9593, 1992a.

Chave, A. D., D. S. Luther, L. J. Lanzerotti, and L. V. Medford, Geoelectric field measurements on a planetary scale: Oceanographic and geophysical applications, *Geophys. Res. Lett., 19*, 1411-1414, 1992b.

Chave, A. D., D. S. Luther, and J. H. Filloux, Observations of the boundary current system at 26.5N in the subtropical North Atlantic Ocean, *J. Phys. Oceanogr., 27*, 1827-1848, 1997.

Cox, C. S., Electromagnetic induction in the oceans an inferences on the constitution of the earth, *Geophys. Surv., 4*, 137-156, 1980.

Cox, C. S., T. Teramoto, and J. H. Filloux, On coherent electric and magnetic fluctuations in the sea, in *Studies on Oceanography*, edited by K. Yoshida, pp.449-457, University of Tokyo Press, Tokyo, 1964.

Cummins, P. F., The barotropic response of subpolar North Pacific to stochastic wind forcing, *J. Geophys. Res., 96*, 8869-8880, 1991.

Cummins, P. F., and H. J. Freeland, Observation and modeling of wind driven currents in the northeast Pacific, *J. Phys. Oceanogr., 23*, 488-502, 1993.

Dickson, R. R., W. J. Gould, P. A. Gurbutt, and P. P. Killworth, A seasonal signal in the ocean currents to abyssal depths, *Nature, 295*, 193-198, 1982.

Duffus, H. J., and N. R. Fowler, On planetary Voltages, ocean tides, and electrical conductivity below the Pacific, *Can. J. Earth Sci., 11*, 873-892, 1974.

Egbert, G. D., Noncausality of the discrete-time magnetotelluric impulse response, *Geophysics, 57*, 1354-1358, 1992.

Faraday, M., Bakerian lecture: Experimental researches in electricity - second series, *Philos. Trans. R. Soc. London, 122*, 163-194, 1832.

Flosadóttir, A. H., J. C. Larsen, and J. T. Smith, Motional induction in North Atlantic circulation models, *J. Geophys. Res., 102*, 10,353-10,372, 1997a.

Flosadóttir, A. H., J. C. Larsen, and J. T. Smith, The relation of seafloor voltages to ocean transports in North Atlantic circulation models: Model results and practical considerations for transport monitoring, *J. Phys. Oceanogr., 27*, 1547-1565, 1997b.

Frankignoul, C., and P. Müller, Quasi-geostrophic response of an infinite β-plane ocean to stochastic forcing by the atmosphere, *J. Phys. Oceanogr., 9*, 104-127, 1979.

Kawatate, K., et al., A cross-spectral analysis of small voltage variation in a submarine cable between Hamada and Pusan with speed variation of the Tsushima warm current, in *Oceanography of Asian Marginal Seas, Elsevier Oceanogr. Ser.*, vol. 54, edited by K. Takano, pp. 207-222, Elsevier Sci., New York, 1991.

Koblinsky, C. J., and P. P. Niiler, The relationship between deep ocean currents and winds east of Barbados, *J. Phys. Oceanogr., 12*, 144-153, 1982.

Lanzerotti, L. J., C. H. Sayres, L. V. Medford, J. S. Kraus, and C. G. Maclennan, Earth potential over 4000km between Hawaii and California, *Geophys. Res. Lett., 19*, 1177-1180, 1992.

Lanzerotti, L. J., A. D. Chave, C. H. Sayres, L. V. Medford, and C. G. Maclennan, Large-scale electric field measurements on the Earth's surface: A review, *J. Geophys. Res., 98*, 23,525-23,534, 1993.

Larsen, J. C., Transport and heatflux of the Florida current at 27°N derived from cross-stream voltages and profiling data: Theory and observations, *Philos. Trans. R. Soc. London, Ser. A, 338*, 169-236, 1992.

Larsen, J. C., and T. B. Sanford, Florida Current volume transports from voltage measurements, *Science, 227*, 302-304, 1985.

Lippert, A., and P. Müller, Direct atmospheric forcing of geostrophic eddies, II, Coherence maps, *J. Phys. Oceanogr., 25*, 106-121, 1995.

Liu, W. T., W. Tang, and P. S. Polito, NASA scatterometer provides global ocean-surface wind fields with more structures than numerical weather prediction, *Geophys. Res. Lett., 25*, 761-764, 1998.

Lizarralde, D., A. D. Chave, G. Hirth, and A. Schultz, Northeastern Pacific mantle conductivity profile from long period magnetotelluric sounding using Hawaii-to-California submarine cable data, *J. Geophys. Res., 100*, 17,837-17,854, 1995.

Longuet-Higgins, M. S., The electric and magnetic effects of tidal streams, *Mon. Not. R. Astron. Soc. Geophys. Suppl., 5*, 285-307, 1949.

Luther, D. S., and A. D. Chave, Observing "integrating" variables in the ocean, in *Proceedings of the 7th 'Aha Huliko'a Hawaiian Winter Workshop on Statistical Methods in Physical Oceanography*, edited by P. Muller and D. Henderson, pp. 103-130, Univ. of Hawaii at Manoa, Honolulu, 1993.

Luther, D. S., A. D. Chave, J. H. Filloux, and P. F. Spain, Evidence for local and nonlocal barotropic responses to atmospheric forcing during BEMPEX, *Geophys. Res. Lett., 17*, 949-952, 1990.

Luther, D. S., J. H. Filloux, and A. D. Chave, Low frequency, motionally induced electromagnetic fields in the ocean, 2, Electric field and Eulerian current comparison, *J. Geophys. Res., 96*, 12,797-12,814, 1991.

Medford, L. V., A. Meloni, L. J. Lanzerotti, and G. P. Gregori, Geomagnetic induction on a transatlantic communications cable, *Nature, 290*, 392-393, 1981.

Mori, T., Variations in the geoelectric field with relation to crustal conditions of the earth, *Geophys. Mag., 42*, 41-104, 1987.

Müller, P., and C. Frankignoul, Direct atmospheric forcing of geostrophic eddies, *J. Phys. Oceanogr., 11*, 287-308, 1981.

Niiler, P. P., and C. J. Koblinsky, A local, time-dependent Sverdrup balance in the eastern North Pacific Ocean, *Science, 229*, 754-756, 1985.

Philander, S. G. H., Forced oceanic waves, *Rev. Geophys., 16*, 15-46, 1978.

Richards, M. L., Tidal signals on long submarine cables, *Ann. Geophys., 33*, 177-178, 1977.

Samelson, R. M., Stochastically forced current fluctuations

in vertical shear and over topography, *J. Geophys. Res.*, *94*, 8207-8215, 1989.

Samelson, R. M., Evidence for wind-driven current fluctuations in the eastern North Atlantic, *J. Geophys. Res.*, *95*, 11,359-11,368, 1990.

Samelson, R. M., and B. Shrayer, Currents forced by stochastic winds with meridionally-varying amplitude, *J. Geophys. Res.*, *96*, 18,425-18,429, 1991.

Sanford, T. B., Motionally induced electric and magnetic fields in the sea, *J. Geophys. Res.*, *76*, 3476-3492, 1971.

Stephenson, D., and K. Bryan, Large scale electric and magnetic fields generated by the Oceans, *J. Geophys. Res.*, *97*, 15,467-15,480, 1992.

Stommel, H., Exploratory measurements of electrical potential differences between widely spaced points in the North Atlantic Ocean, *Arch. Meteorol. Geophys. Bioklimatol., Ser. A*, *7*, 292-304, 1954.

Teramoto, T., Estimation of sea-bed conductivity and its influence upon velocity measurements with towed electrodes, *J. Oceanogr. Soc. Jpn.*, *27*, 7-18, 1971.

Teramoto, T., and H. Kojima, Education of hydrodynamical processes from cross-channel electric-potential differences in the Kuroshio area around the Izu ridge, *J. Oceanogr.*, *50*, 339-363, 1994.

Thomson, D. J., Spectrum estimation and harmonic analysis, *Proc. IEEE*, *70*, 1055-1096, 1982.

Tyler, R.H., and L.A. Mysak, Motionally-induced electromagnetic fields generated by idealized ocean currents, *Geophys. Astrophys. Fluid Dyn.*, *80*, 167-204, 1995.

Widrow, B. and S. D. Stearns, *Adaptive Signal Processing*, 474 pp., Prentice-Hall, Englewood Cliffs, N.J., 1985.

Willeband, J. S., G. H. Philander, and R. C. Pacanowski, The oceanic response to large scale atmospheric disturbances, *J. Phys. Oceanogr.*, *10*, 411-429, 1980.

A. D. Chave, Woods Hole Oceanographic Institution, Woods Hole, MA 02543. (e-mail: achave@whoi.edu)

I. Fujii, Earthquake Research Institute, University of Tokyo, Yayoi 1-1-1, Bunkyo-ku, Tokyo, 113-0032, Japan. (e-mail: fujii@utada-sun.eri.u-tokyo.ac.jp)

(Received February 12, 1998; revised July 10, 1998; accepted August 10, 1998.)